Stanford Exploration Project, Report 115, May 22, 2004, pages 81–89

Short Note

Improving the amplitude accuracy of downward continuation operators (Part 2)

Ioan Vlad and Thomas Tisserant[1]

INTRODUCTION

One-way wavefield continuation methods correctly account for traveltimes, but the amplitude and phase of the images they produce can still be improved. Zhang et al. (2002; 2003a; 2003b) present theoretical formulations of amplitude-improving corrections for shot-profile migration. Vlad et al. (2003) show concrete ways of implementing Zhang's theory for both finite-difference and mixed-domain extrapolators, with applications to constant-velocity, laterally smooth and heterogeneous cases.

The above-described corrections consist of two parts: one that is applied at the $z = 0$ boundary, and one that is applied in the propagation operator. The boundary condition correction depends only on the velocity at the surface, while the propagation correction takes the entire interval velocity model into account and is directly proportional to its vertical gradient, v_z, vanishing where this becomes zero. As a result, the effect of the boundary condition correction can be tested in isolation, using constant velocity models. Figure 1 in Vlad et al. (2003) shows that the Zhang boundary condition correction improves the phase and brings the amplitudes very close to the ones computed analytically, especially in the case of the mixed-domain implementation. Valenciano et al. (2004) show the effect of applying it to propagation through the Marmousi model. They also present a more intuitive interpretation of the boundary condition correction, and an alternative method for computing it.

Vlad et al. (2003) show in their Figure 2 that the propagation operator correction is equivalent to the WKBJ one in a $v(z)$ medium. They also apply it to the $v(x,z)$ model presented in Figure 3 of their paper. However, the results (their Figure 4) did not show a visible effect of the correction. In the first section that follows, we explain why that was the case for that very particular velocity model, and we quantitatively show that the propagation operator correction does have visible effects. In the last section of this paper, we discuss the application of the Zhang corrections to the linearized downward continuation operator used in wave equation migration velocity analysis.

[1]**email:** nick@sep.stanford.edu, thomas@sep.stanford.edu

APPLICATION TO PROPAGATION IN A MORE GENERAL $V(X,Z)$ MODEL

The velocity model used by Vlad et al. (2003) for examining the effects of the amplitude corrections was particularly unsuitable for the problem. It belonged actually to a limit case in which the amplitude corrections canceled themselves. We will show below why that was the case and we will analyze the effects of the corrections by picking amplitudes at each midpoint in a wavefield depth slice.

At each downward continuation step, the propagation amplitude correction applied to the wavefield is:

$$P'_z = P_z e^{-\frac{v_z \Delta z}{2v(x,z)} \frac{1}{1-\left[\frac{v(x,z)k_x}{\omega}\right]^2}}, \tag{1}$$

where v_z denotes the vertical gradient of the velocity. When variations of velocity in the x direction exist, this exponential is strictly noncommutative with the downward continuation step. The noncommutativity however becomes weak in the particular case when the laterally varying velocity is symmetrical with respect to a horizontal plane. In the case of such symmetry, corrections of the same magnitude along midpoint, but of different sign (because of an opposing sign for v_z) cancel each other. The corrections in the lower half of the velocity model in Figure 3 of Vlad et al. (2003) were therefore erasing the effects of the ones performed in the upper half. As a result, Figure 4 of Vlad et al. (2003) was not showing any results of the correction.

Recognizing that such a symmetrical configuration is not very plausible geologically, we downward continued (with split-step) only through the upper half of the respective velocity model. This half is depicted in Figure 1. The top panels in Figure 2 show the wavefield at a depth of 1000m. The four panels represent all the combinations of applying ("+") or not ("-") the boundary condition correction ("L") and/or the propagation correction ("G"). The lower half of the figure shows the maximum amplitudes picked for each midpoint. The effect of the propagation correction (Curves "-L+G" and "+L+G") is visible now as increased focusing and reduced amplitude decay with offset. The boundary condition correction (Curves "+L-G" and "+L+G") also has a strong effect; it especially diminishes the amplitude decay. We expect the two Zhang corrections to increase, when cummulated, power for large dips and for large incidence angles on the reflector.

APPLICATION TO LINEARIZED DOWNWARD CONTINUATION

Linearized downward continuation – purpose and description

Let us define a slowness perturbation $\Delta s = s - s_0$ as a difference between two slowness models, one of which (s_0) is named the "background slowness". By undertaking several approximations, the most notable of which is Born, the mixed-domain downward continuation operator can be written as an explicit function of the slowness perturbation. This allows an explicit relation between the slowness perturbation and the wavefield. In conjunction with the imaging

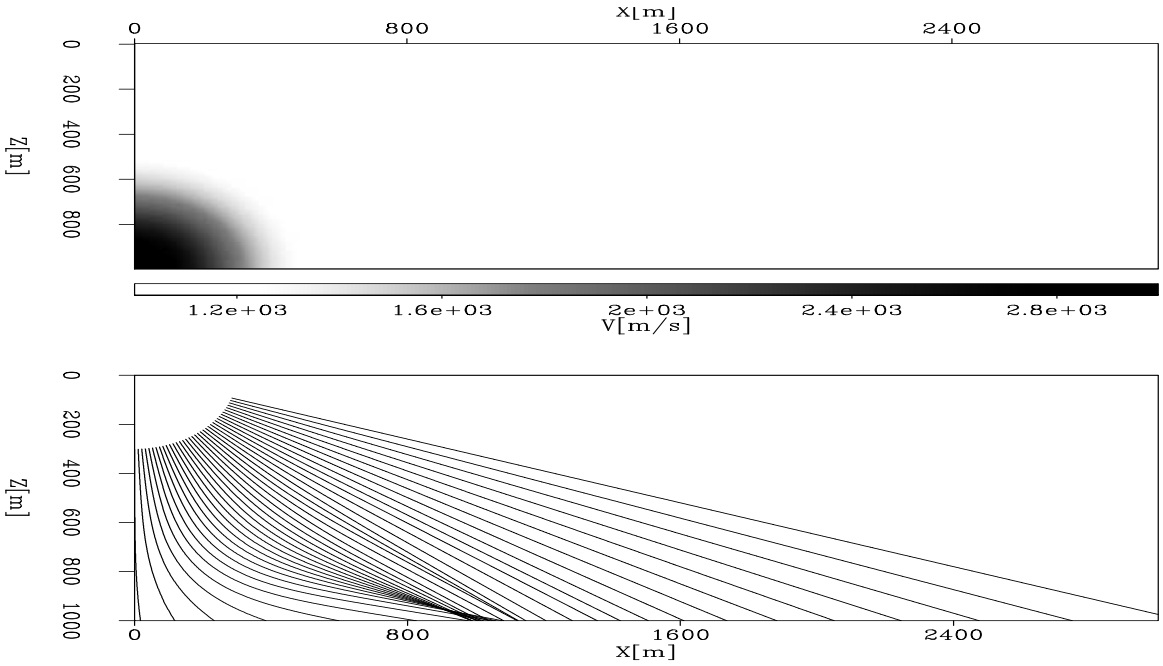

Figure 1: **Top panel:** Upper half of the velocity model used by Vlad et al. (2003). Figure 2 shows the amplitudes produced by propagation through this velocity model. **Bottom panel:** Rays shot from $(0,0)$, shown for an enhancement of the intuitive appreciation of the focusing during the propagation. nick3-g1 [CR]

condition, this allows writing an explicit relation between the slowness perturbation and the image. This relation is the basis of Wave-Equation Migration Velocity Analysis (WEMVA), a complete flowchart of which is presented in Figure 3. This procedure finds the velocities in the following way: using the recorded data and the background slowness, it creates a background image. This image is then improved so that it is closer to the optimally focused one, then the two images are subtracted to create an image perturbation. This is transformed into a wavefield perturbation through an inverse imaging condition, then is upward continued, to create an adjoint scattered wavefield. This in turn is transformed into a slowness update by inverting the linearized downward continuation operator. This operator is linearized so that its inversion will be computationally cheap. A complete derivation is provided by Biondi and Sava (1999), with more explanations in Sava (2000).

If we denote the wavefield as U, the linearized downward continuation (complexified local Born-Fourier method), according to Appendix B in Vlad (2002), is given by:

$$U_{z=n\Delta z} = \left(\prod_{1}^{n} \mathcal{T}\right) U_{z=0} + \sum_{j=1}^{n} \left[\left(\prod_{1}^{n-j} \mathcal{T}\right) \not{s} \Delta s_{z=j\Delta z} \left(\prod_{1}^{j} \mathcal{T}\right) U_{z=0} \right], \tag{2}$$

where $\mathcal{T}$ is the background wavefield downward continuation operator:

$$\mathcal{T} = e^{i\Delta z \sqrt{\omega^2 s_o{}^2 - (1-i\eta)^2 |\mathbf{k_m}|^2}}, \tag{3}$$

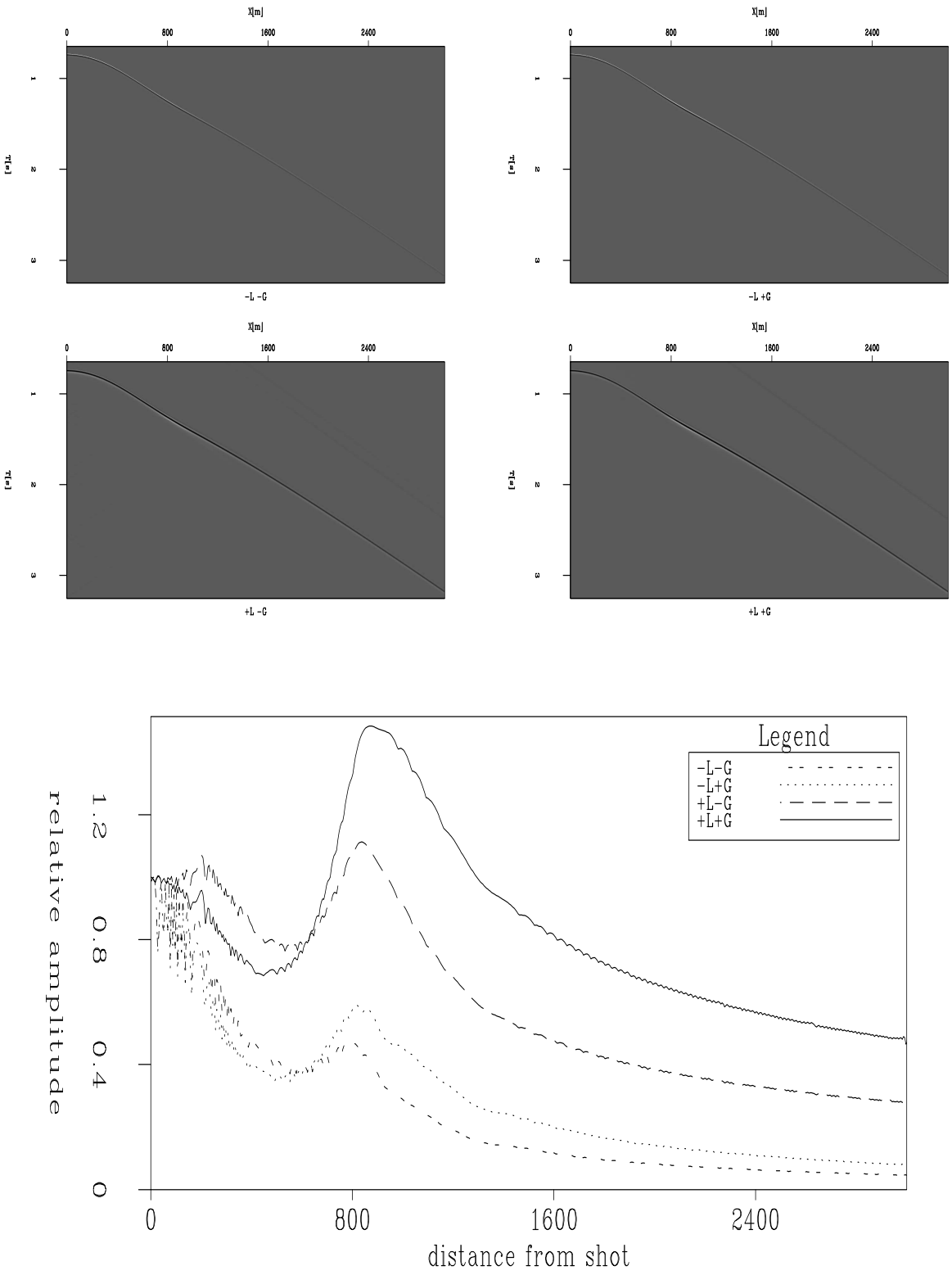

Figure 2: “L” denotes the boundary condition correction, “G” denotes the propagation correction, a "+” shows that the respective correction was applied, and a “-” shows that it was not. **Top panels:** Wavefield generated by a shot at (0,0) in the velocity model from Figure 1, and recorded at the bottom of that velocity model. **Bottom panel:** Maximum amplitudes picked for each x location in the top panels. nick3-g2 [CR]

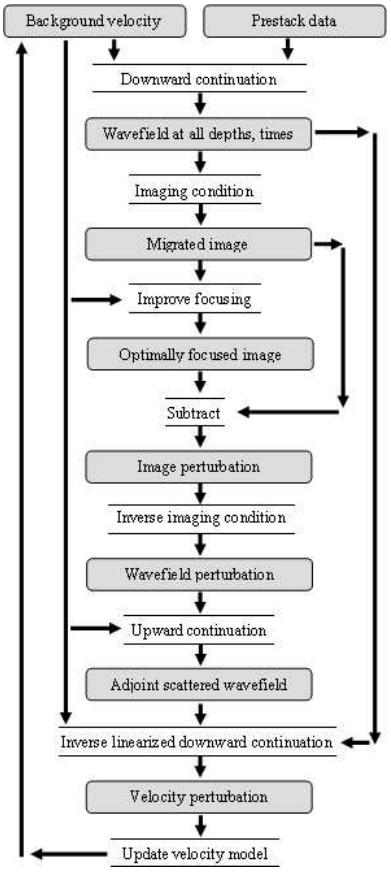

Figure 3: WEMVA flowchart, provided for illustrating the use of linearized downward continuation. nick3-wemva [NR]

and $\mathcal{S}$ is the scattering operator:

$$\mathcal{S} = \frac{i\,\Delta z \omega^2 s_o}{\sqrt{\omega^2 {s_o}^2 - (1 - i\,\eta)^2 |\mathbf{k_m}|^2}}. \tag{4}$$

The boundary condition correction

We tested the amplitude correction at the boundary condition by downward propagating a shot and picking the amplitudes of the wavefield recorded at a certain depth. Since our particular purpose of using WEMVA is finding velocity anomalies that generate focusing-effect AVO (Vlad and Biondi, 2002), we used the same focusing-generating velocity model as that presented in the lower right panel of Figure 6 of Vlad (2002). For convenience, we present it in the upper panel of Figure 4, also tracing wavefronts through it for a better visualization of the kinematics of propagation. The time delays induced by the presence of the low-velocity slab have not been shown because they are under the common picking threshold – this is a typical focusing-effect AVO case.

To obtain the curves in the lower panel of Figure 4, for each of the three methods, we propagated a wavefield through the velocity model in the upper panel of the figure (with the low-velocity slab), and another wavefield through the constant-velocity background only. For

each x location, we picked the maximum amplitudes of each wavefield at the depth of 6000m, and we divided the amplitudes obtained from the model with the slab by the amplitudes obtained from the constant-velocity background. A deviation from the value of 1 indicates the presence of the wavefield scattered by the slab. We performed this procedure using three different algorithms: (1) – Linearized downward continuation with no amplitude correction applied; (2) – Linearized downward continuation with boundary condition amplitude correction applied at the surface; (3) – Pseudospectral wave propagation (Biondi, 2002), for reference. The application of the boundary condition correction has brought the values closer to those of the reference curve. A possible shot-profile formulation of WEMVA would therefore benefit from the application of the boundary condition correction.

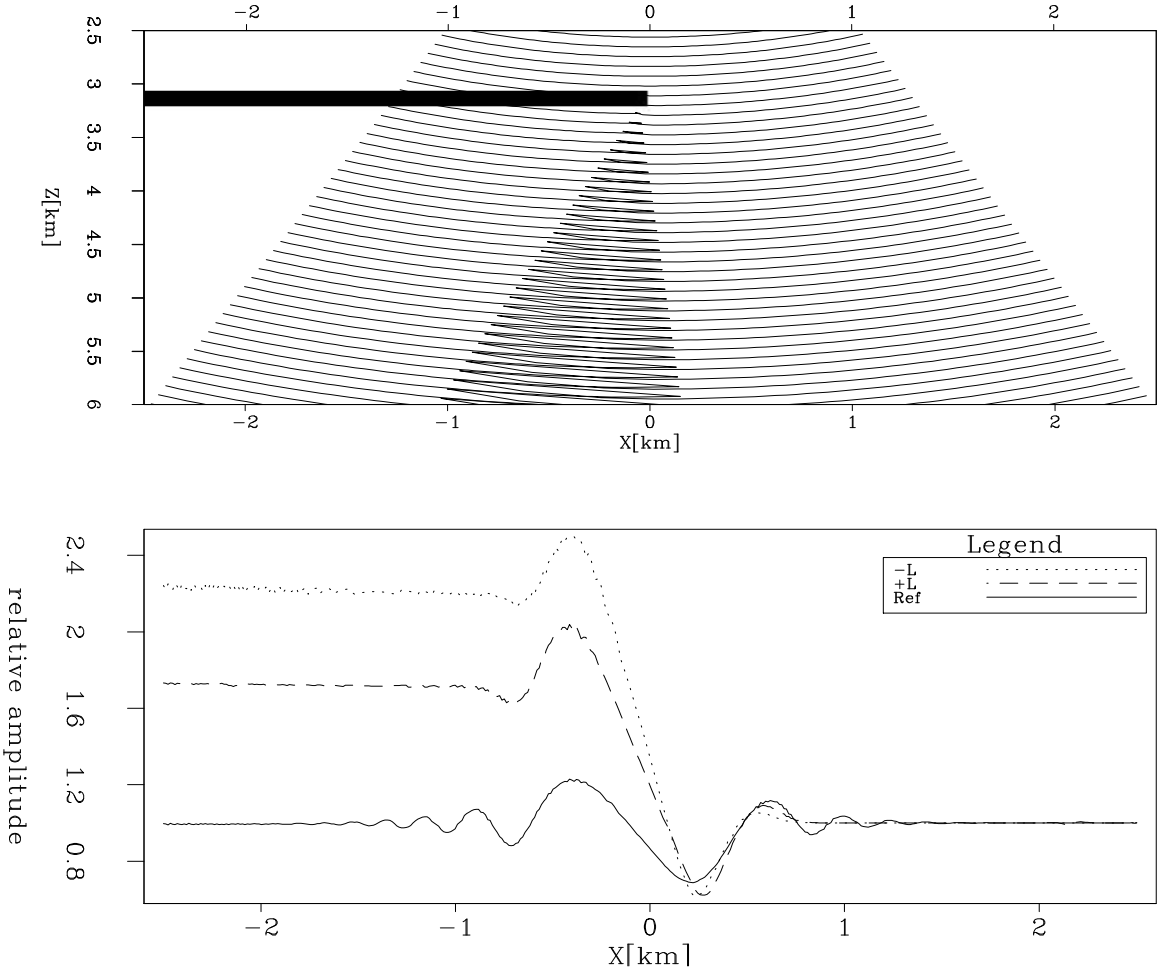

Figure 4: **Top panel:** Velocity model for testing the amplitude behavior of the linearized downward continuation operator. A shot has been generated at (0,0) and the wavefield is recorded at a depth of 6 km. The thin slab has a velocity of 1647 m/s, contrasting to the background of 1830 m/s. Wavefronts have been traced for better visualization of propagation kinematics. **Bottom panel:** Curve "-L" – Linearized downward continuation with no amplitude correction applied; Curve "+L" – Linearized downward continuation with boundary condition amplitude correction; Curve "Ref" – Pseudospectral wave propagation. nick3-g3 [CR]

The propagation operator correction

Things are different, however, for the amplitude correction which is applied during the propagation. Equation 28 of Vlad et al. (2003) states that the correction to be applied at each downward continuation step is

$$U_z' = U_z e^{-\frac{v_z \Delta z}{2v}} \left[1 - \frac{v_z \Delta z v}{2} \left(\frac{k_x}{\omega} \right)^2 + \frac{v_z \Delta z v^2}{2} \left(\frac{v_z \Delta z}{4} - v \right) \left(\frac{k_x}{\omega} \right)^4 \right]. \tag{5}$$

Counting a possible linearization of the exponential in front and the presence of v_z, this is an expression of degree 5 in velocity. Moreover, at each depth step this has to be multiplied with the first-order-in-slowness propagation step in Equation 2 . The result would be a expression of at least degree 6. Discarding terms of order higher than 1 would result in losing an important amount accuracy in the propagation step itself, since a part of it will be multiplied with higher-order amplitude correction terms. We conclude that the propagation operator amplitude correction is not applicable to linearized downward continuation because of compounding linearization errors that will affect both the kinematics and the amplitudes.

CONCLUSIONS

We continue the work of Vlad et al. (2003) on implementing the Zhang amplitude corrections for wavefield extrapolation imaging. We apply the corrections to the case of propagation through a less particular $v(x,z)$ velocity model than the one used in the previous paper. The corrections result in an increase in wavefield focusing. We apply with encouraging results the boundary condition correction to the linearized downward continuation used in wave-equation migration velocity analysis. The propagation operator correction, however, is not applicable to linearized downward continuation.

ACKNOWLEDGMENTS

We thank Guojian Shan for performing the pseudospectral wave modeling used in Figure 4.

REFERENCES

Biondi, B., and Sava, P., 1999, Wave-equation migration velocity analysis: SEP–**100**, 11–34.

Biondi, B., 2002, Reverse time migration in midpoint-offset coordinates: SEP–**111**, 149–157.

Sava, P., 2000, A tutorial on mixed-domain wave-equation migration and migration velocity analysis: SEP–**105**, 139–156.

Valenciano, A. A., Tisserant, T., and Biondi, B., 2004, Surface boundary condition for one-way wave equation shot-profile migration: SEP–**115**, 71–80.

Vlad, I., and Biondi, B., 2002, Velocity estimation for seismic data exhibiting focusing-effect avo: SEP–**111**, 107–123.

Vlad, I., Tisserant, T., and Biondi, B., 2003, Improving the amplitude accuracy of downward continuation operators: SEP–**113**, 163–176.

Vlad, I., 2002, Velocity estimation for seismic data exhibiting focusing-effect AVO (part 2): SEP–**112**, 47–64.

Zhang, Y., Sun, J., Gray, S. H., Notfors, C., Bleinstein, N., and Zhang, G., 2002, True amplitude migration using common-shot one-way wavefield extrapolation:, *in* 64th EAGE Annual Conference.

Zhang, Y., Zhang, G., and Bleinstein, N., 2003a, Theory of true amplitude common-shot migration:, *in* 65th EAGE Annual Conference.

Zhang, Y., Zhang, G., and Bleinstein, N., 2003b, Theory of true amplitude one-way wave equations and true amplitude common-shot migration:, *in* 65th EAGE Annual Conference.